Fluid - Soil - Structure Interaction of a Circular Bridge Pier Column

by

W. Phillip Yen, Ph.D., P.E [1] and Kornel Kerenyi, Ph.D. [2]

ABSTRACT

The goal of this research is to test various combinations of hazards such as wind, flood, scour and dynamic loadings (e.g., earthquakes and vessel impacts) for impacts to bridge pier structural stability. Most equations and design criteria currently in use treat these hazards separately, although they can occur concurrently. A study that combines all hazards and dynamic loadings would be very complicated. Therefore the initial research is designed and fabricated to study only flow (flood), soil (sediment particle size and river bed geometry) and dynamic loading (harmonic, random and impulsive loads). A rigid mass, single degree of freedom (SDOF) oscillator represents the simplified bridge pier. A specially designed flume, which is 3000 mm long and 400 mm wide, allows for the investigation of different soil conditions and various flow velocities. The oscillating pier is mounted elastically on a structure over the test section of the flume. Two synchronous linear drive motors apply the dynamic loads. The oscillating bridge pier, neglecting flow and soil conditions, represents a perfect linear spring-damper system. In combination with flow and soil the system gets nonlinear. The goal of this initial research is to replace the soil and flow effects with an equivalent spring-damper system. This paper summarizes soil-structure interaction and fluid-soil-structure interaction tests. The equivalent spring and damping coefficients are plotted vs. forcing frequencies.

KEYWORDS: multi hazard impacts on bridge piers, fluid-soil- structure interaction, soil-structure interaction

1.0 INTRODUCTION

This study is concerned with the safety of bridges subjected to different natural hazard events. The events of interest are earthquakes, scour, hurricanes and vessel impact. Several bridge foundations are under water, so the structural response during an earthquake under these combined conditions is very complicated. Research at the Federal Highway Administration (FHWA) Turner Fairbanks Highway Research Center (TFHRC) Seismic Hazard Mitigation has focused on developing an experimental set-up to investigate a simple model where flow (fluid), scour (soil) and earthquakes (dynamic forces) interact with a bridge pier structure.
The experimental set-up is designed to study the fluid-soil interaction of a rigid single degree of freedom (SDOF) oscillator using a forced oscillation experiment. The linear SDOF oscillator acts as a reference system to investigate the nonlinear behavior of the system when it interacts with fluid and soil. The identification procedure to determine the additional fluid and soil forces based on a forced oscillation test are similar used to identify fluid dynamic damping and stiffness. Staubli (1983) and Deniz (1997) used forced oscillation tests in a tow-tank to determine force coefficients and phase angle to describe the fluid dynamic system. Bardowicks (1976) proposed a description of flow-induced load in the form of components in phase with body displacement and velocity. They use controlled vibration experiments in a wind tunnel. Kerenyi and Yen (2002, 2003 and 2004) use forced oscillation tests to investigate fluid-structure and soil-structure

[1] Research Structural Engineer, Seismic Hazard Mitigation (HRDI-07), Federal Highway Administration, 6300 Georgetown Pike, McLean, Virginia 22101; PH (202) 493-3056; FAX (202) 493-3442; email: wen-huei.yen@fhwa.dot.gov
[2] Hydraulic Research Engineer, GKY and Associates, Inc., 5411-E Backlick Road, Springfield, Virginia 22151; PH (703) 642-5080; FAX (703) 642-5367; email: kornel.kerenyi@fhwa.dot.gov

interaction and to model fluid and soil with an equivalent spring damper system.

2.0 EXPERIMENTAL SET-UP

The experimental set-up consists of two major subsystems: a flume to simulate various flow and riverbed conditions and the shaking device to apply different dynamic loadings.

2.1 Flume

The flume consists of a 1300 mm long inlet and a 2000 mm straight channel (Figure 1). The upstream flow conditioning is achieved using filter mats, a honeycomb flow straightener, and a carefully designed trumpet-shaped inlet. The flume is designed to have a uniform flow distribution over the width and to have fully developed turbulent flow (following Prandtl's velocity distribution) at the test section. The recess at the test section is 400 mm x 300 mm (length x width) and 80 mm deep, and can be filled with sand particles of various sizes. The roughness of the fixed bed upstream of the recess can be varied according to the sand particles used in the recess. A 25 l/s pump provides the flume with water, which is stored under the flume in a water tank. A flow meter measures the discharge and an ultra sonic flow depth meter determines the flow depth. A laser distance meter, which is mounted on a portal robot, can scan scour holes during test runs. The flow velocity is measured with an electro magnetic velocity probe.

2.2 Shaking device and bridge pier model

The shaking device (Figure 2) is mounted above the flume on a rigid frame at the test section. The rigid frame with shaker can be turned 90 degrees and is portable. Two synchronous linear drive motors apply dynamic forces up to 12 Hz. Band limited random noise can be used to simulate earthquake-loading. A ridged model bridge pier is fixed to a platform with linear bearings, which is attached to a linear guide system and mounted elastically to the drive platform. Using different coil springs for the elastical support can vary the natural frequency. The mechanical (structural) subsystem represents a linear SDOF system, which is lightly damped to study a significant peak resonant response. The damping ratio is determined by the Half-Power (Band-Width) method. An electro magnetic damper is used to vary the damping of the SDOF. The other end of the vertical rigid model pier is mounted in soil to interact with the soil subsystem or fluid soil subsystem. The body response displacement is measured with a laser distance meter and the response acceleration with accelerometers. The response velocity is determined by integrating the response acceleration. Two load cells measure the applied dynamic loading. The circular bridge pier is modeled using a vertical mounted aluminum rod with 20 mm OD.

2.3 Dynamic properties of the linear SDOF oscillator

As shown in Figure 3, the equilibrium of forces can be written

$$f_I(t) + f_D(t) + f_S(t) = 0 . \qquad (1)$$

Substituting for inertial, damping, and elastic forces in equation 1 yields

$$m\ddot{v}_T(t) + c\dot{v}_T(t) + k\,v(t) = 0 . \qquad (2)$$

Before this equation can be solved, all forces must be expressed in terms of a single variable, which can be accomplished by noting the total motion as follows

$$v_T(t) = v(t) + v_G(t). \qquad (3)$$

Substituting equation (3) into equation (2) leads to the equation of motion, since the motor displacement represents the specified dynamic input to the structure

$$m\ddot{v}_T(t) + c\dot{v}_T(t) + k v_T(t) = k v_G(t) = p(t). \qquad (4)$$

The dynamic properties can be determined based on the balance of forces acting on the linear mass oscillator under steady state harmonic condition whereby the total response is

$$v_T(t) = \rho_T \exp[\mathrm{i}(\overline{\omega} t - \theta)]. \qquad (5)$$

Force equilibrium requires that the sum of the inertial $f_I(t)$, damping $f_D(t)$ and spring forces $f_S(t)$ equal the applied load.

These forces are

$$f_I(t) = m\ddot{v}(t) = -m\overline{\omega}^2 \rho_T \exp[i(\overline{\omega} t - \theta)], \qquad (6)$$

$$f_D(t) = c\dot{v}(t) = i c \overline{\omega} \rho_T \exp[i(\overline{\omega} t - \theta)], \qquad (7)$$

$$f_S(t) = k v(t) = k \rho_T \exp[i(\overline{\omega} t - \theta)]. \qquad (8)$$

These forces, along with the applied loading, are shown as vectors in the complex plane (Figure 4) also shown is the closed polygon of forces required for equilibrium in accordance with equation (4)

$$f_I + f_D + f_S = p(t). \qquad (9)$$

Inertial, damping, and spring forces as given in equation (6) to (8) are in phase with the acceleration, velocity, and displacement motions, respectively. Equating the real part and the imaginary part of the vectors in the complex plane shown in Figure 4 results in

$$m = \frac{k\rho_T - k\rho_G \cos\theta}{\overline{\omega}^2 \rho_T} \qquad (10)$$

and

$$c = \frac{k\rho_G \sin\theta}{\overline{\omega}\rho_T}. \qquad (11)$$

Knowing the phase angle between body response displacement and applied dynamic force and the stiffness of the linear SDOF oscillator one can compute mass and damping coefficient based on equations (10 and 11). The stiffness was determined experimentally using a static force –displacement relationship. The dynamic properties are listed in Table 1.

3.0 MATHEMATICAL BACKGROUND

The objective of this research is to replace fluid and soil with an equivalent spring damper system and to study the non-linear behavior of the fluid and soil stiffness and damping coefficients (Figure 5). To examine these properties only movements relative to the ground displacements are considered (Figure 6).

3.1 Soil - Structure Interaction

The identification procedure of the soil-structure interaction (Figure 7) is based on the idea of a forced oscillation experiments to determine soil stiffness and damping. Additional damping and stiffness forces can model the soil subsystem (equation 12), which are functions of amplitude and frequency.

$$f_I + f_D + f_S + f_{S-S} + f_{D-S} = p(t)\,. \qquad (12)$$

The soil tests described here only the exciting frequency $\overline{\omega}$ and the amplitude ρ was varied. Non-cohesive soil with $D_{50} = 0.3$ mm was used for the soil – structure experiments. The pile depth d (Figure 7) was constant at the beginning of each test. These soil forces are frequency and amplitude dependent as shown in equations (13) and (14)

$$f_{S-S}(t) = k_S(\rho_T, \overline{\omega})\, v_T(t) = k_S(\rho_T, \overline{\omega})\, \rho_T \qquad (13)$$

and

$$f_{D-S} = c_S(\rho_T, \overline{\omega})\, \dot{v}_T(t) = i\, c_S(\rho_T, \overline{\omega})\, \overline{\omega}\, \rho_T\,. \qquad (14)$$

Inserting equation (13) and (14) into equation (12) leads to

$$\begin{aligned} & m\, \ddot{v}_T(t) + c\, \dot{v}_T(t) + k\, v_T(t) + \\ & + c_S(\rho_T, \overline{\omega})\, \dot{v}_T(t) + k_S(\rho_T, \overline{\omega})\, v_T(t) \\ & = k\, \rho_G \exp(\mathrm{i}\, \overline{\omega}\, t). \end{aligned} \qquad (15)$$

To determine these additional forces cross power spectrum is used to compute the phase angle θ between body response displacement amplitude ρ_T and applied dynamic force amplitude $k\rho_G$. The forces can be expressed by equilibrating the dynamic force components (Figure 8).

$$f_{S-F} = k\, \rho_G \cos\theta - f_S - f_I \qquad (16)$$

$$f_{D-F} = k\, \rho_G \sin\theta - f_D\,. \qquad (17)$$

Substituting equations (6) to (8) and equations (13) and (14) into equation (16) and (17), one obtains the soil coefficient functions

$$k_S(\rho_T, \overline{\omega}) = \frac{k(\rho_G \cos\theta - \rho_T) + \overline{\omega}^2 \rho_T m}{\rho_T} \qquad (18)$$

$$c_S(\rho_T,\overline{\omega}) = \frac{k\,\rho_G \sin\theta - \overline{\omega}\,\rho_T c}{\overline{\omega}\,\rho_T}. \qquad (19)$$

3.2 Fluid - Soil - structure interaction

To describe the fluid-soil subsystem (Figure 9) again an equivalent damping and stiffness force will be identified. The additional fluid-soil forces are plotted in the complex plane as shown in Figure 10. Equilibrating the forces results in

$$f_I + f_D + f_S + f_{S-FS} + f_{D-FS} = p(t). \qquad (20)$$

The fluid-soil tests described here (Figure 11) the exciting frequency $\overline{\omega}$ and the amplitude ρ was varied. Non-cohesive soil with D_{50} = 0.3 mm and a still water depth of 100 mm was used for the fluid-soil tests. The pile depth *d* (Figure 9) was constant at the beginning of each test. These fluid-soil forces are again frequency and amplitude dependent as shown in equations (21) and (22)

$$f_{S-FS}(t) = k_{FS}(\rho_T,\overline{\omega})\,v_T(t) = k_{FS}(\rho_T,\overline{\omega})\,\rho_T \qquad (21)$$

and

$$f_{D-FS} = c_{FS}(\rho_T,\overline{\omega})\,\dot{v}_T(t) = i\,c_{FS}(\rho_T,\overline{\omega})\,\overline{\omega}\,\rho_T. \qquad (22)$$

Inserting equation (21) and (22) into equation (20) leads to

$$\begin{aligned} &m\,\ddot{v}_T(t) + c\,\dot{v}_T(t) + k\,v_T(t) + \\ &+ c_{FS}(\rho_T,\overline{\omega})\,\dot{v}_T(t) + k_{FS}(\rho_T,\overline{\omega})\,v_T(t) \\ &= k\,\rho_G \exp(i\,\overline{\omega}\,t). \end{aligned} \qquad (23)$$

Cross power spectrum is used to calculate the phase angle θ between body response displacement amplitude ρ_T and dynamic force amplitude $k\rho_G$. Equilibrating the real and imaginary components of the forces (Figure 10) results in

$$f_{S-FS} = k\,\rho_G \cos\theta - f_S - f_I \qquad (24)$$

$$f_{D-FS} = k\,\rho_G \sin\theta - f_D. \qquad (25)$$

Substituting equations (6) to (8) and equations (21) and (22) into equation (24) and (25), to get the fluid-soil coefficient functions

$$k_{FS}(\rho_T,\overline{\omega}) = \frac{k\,(\rho_G\cos\theta - \rho_T) + \overline{\omega}^2\rho_T m}{\rho_T} \qquad (26)$$

$$c_{FS}(\rho_T,\overline{\omega}) = \frac{k\,\rho_G \sin\theta - \overline{\omega}\,\rho_T c}{\overline{\omega}\,\rho_T}. \qquad (27)$$

4.0 RESULTS

The soil stiffness coefficients and soil damping coefficients vs. exiting frequencies are plotted in Figures 12 and 13 for four different amplitudes (ρ_{T1} = 2.5 mm, ρ_{T2} = 3.0 mm, ρ_{T3} = 3.5 mm and ρ_{T4} = 4.0 mm). Both charts indicate a nearly linear decay in soil stiffness and soil damping with increasing forcing frequencies. This indicates that the soil softens with increasing the exiting frequency.
In Figures 14 and 15 the fluid-soil stiffness and fluid-soil damping coefficients are plotted for four different amplitudes (ρ_{T1} = 2.5 mm, ρ_{T2} = 3.0 mm, ρ_{T3} = 3.5 mm and ρ_{T4} = 4.0 mm) vs. forcing frequencies. Also in this case the charts show a nearly linear decay in fluid-soil stiffness and fluid-soil damping with increasing forcing frequencies. It is interesting to observe that the fluid-soil stiffness is higher and the fluid-soil damping lower compared to the soil-stiffness and soil damping for the analyzed amplitudes. Adding fluid to the cohesive soil reduces the damping properties and increases the stiffness of the fluid-soil-structure system.

6.0 REFERENCES

Deniz S., Staubli T., (1997), Oscillating rectangular and octagonal profiles: Interaction of leading- and trailing-edge vortex formation, Journal of Fluids and Structures, Vol. 11, p. 3-31.

Barowicks, H., (1976), Effects of cross-sectional shape and amplitude on aeroelastic vibrations of sharp-edged prismatic bodies, Doctoral Dissertation, Techn. Universitaet Hannover, Germany.

Kerenyi K., Yen P. W., (2002), Multi Hazard Dynamic Testing for Bridge Piers, Proceedings of the 18th US-Japan Bridge Engineering Workshop, St Luis, Missouri, p. 77-82.

Kerenyi K., Yen P. W., (2003), Rocking Motion of a Bridge Foundation Platform, Proceedings of the 19th US-Japan Bridge Engineering Workshop, Tsukuba Science City, Japan

Kerenyi K., Yen P. W., (2004), Fluid - Structure and Soil - Structure Interaction of Bridge Piers, Proceedings of the 36th UJNR- Joint Meeting United States – Japan Panel on Wind and Seismic Effects, Gaithersburg, Maryland

Staubli, T., (1983), Investigation of oscillating forces on a vibrating cylinder in cross-flow, Doctoral Dissertation, ETH Zuerich, Switzerland

Mass	1668 g
Stiffness	1570 N/m
Damping ratio	5.54 %
Natural frequency	4.85 Hz

Table 1: Dynamic properties of the linear SDOF oscillator

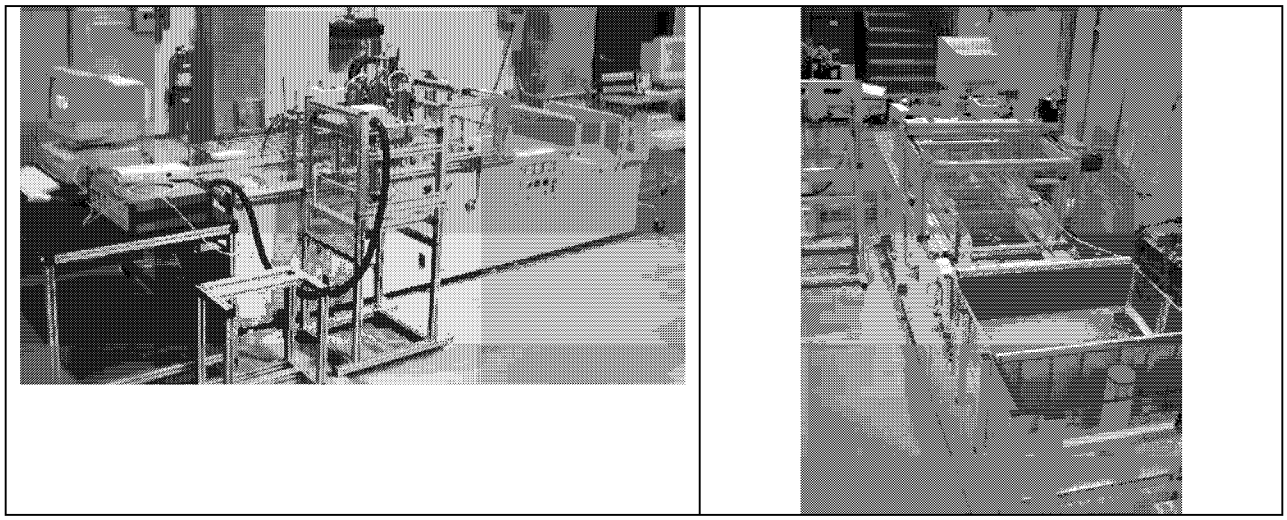

Figure 1. Test flume, trumpet shaped inlet and Multi-Hazard Lab

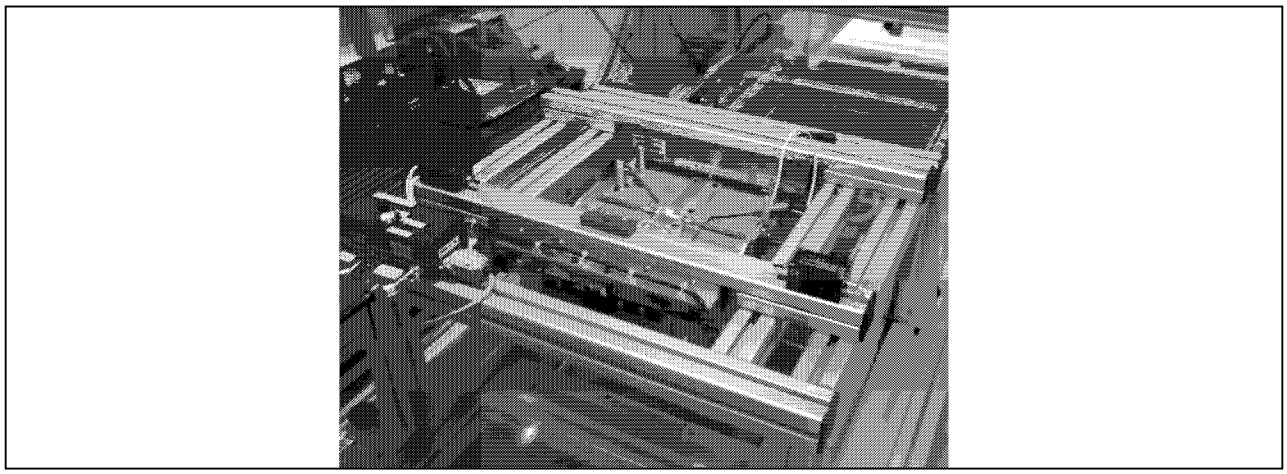

Figure 2: Shaking device

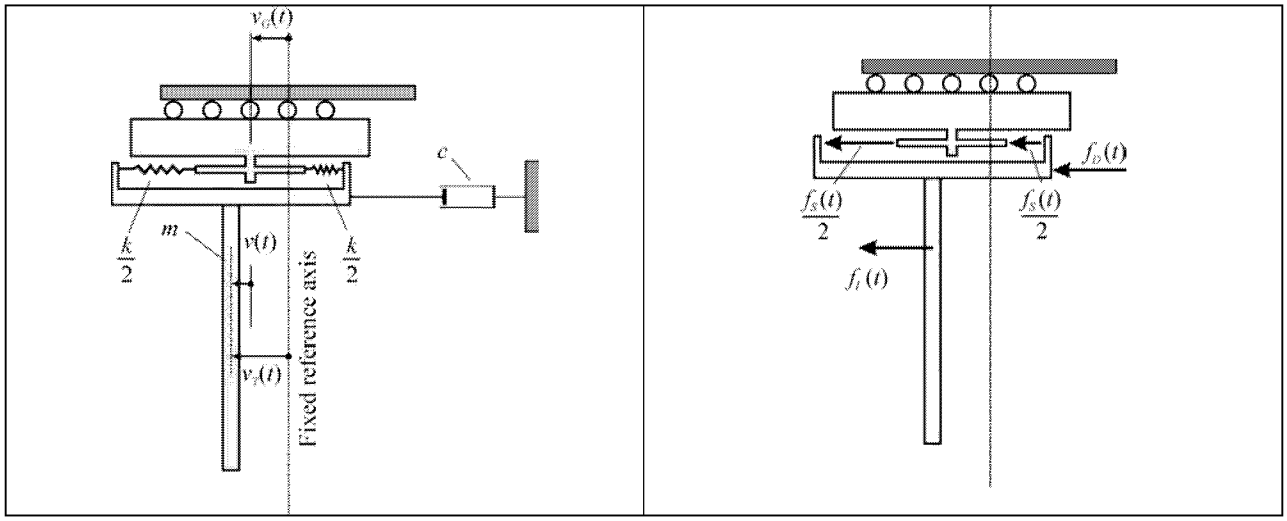

Figure 3: Linear SDOF system showing motion of system and equilibrium of forces

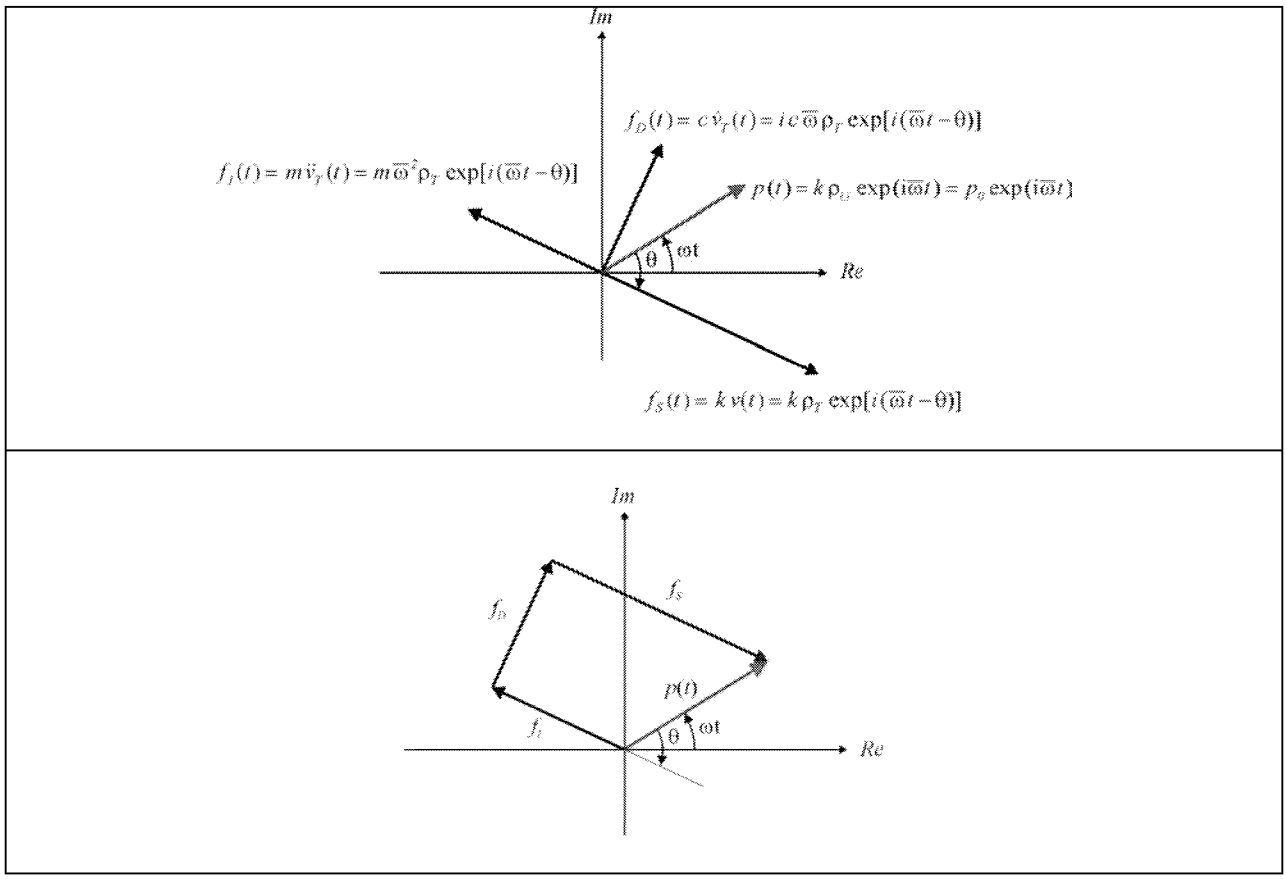

Figure 4: Steady state harmonic forces using viscous damping in a complex plane representation and closed force polygon representation

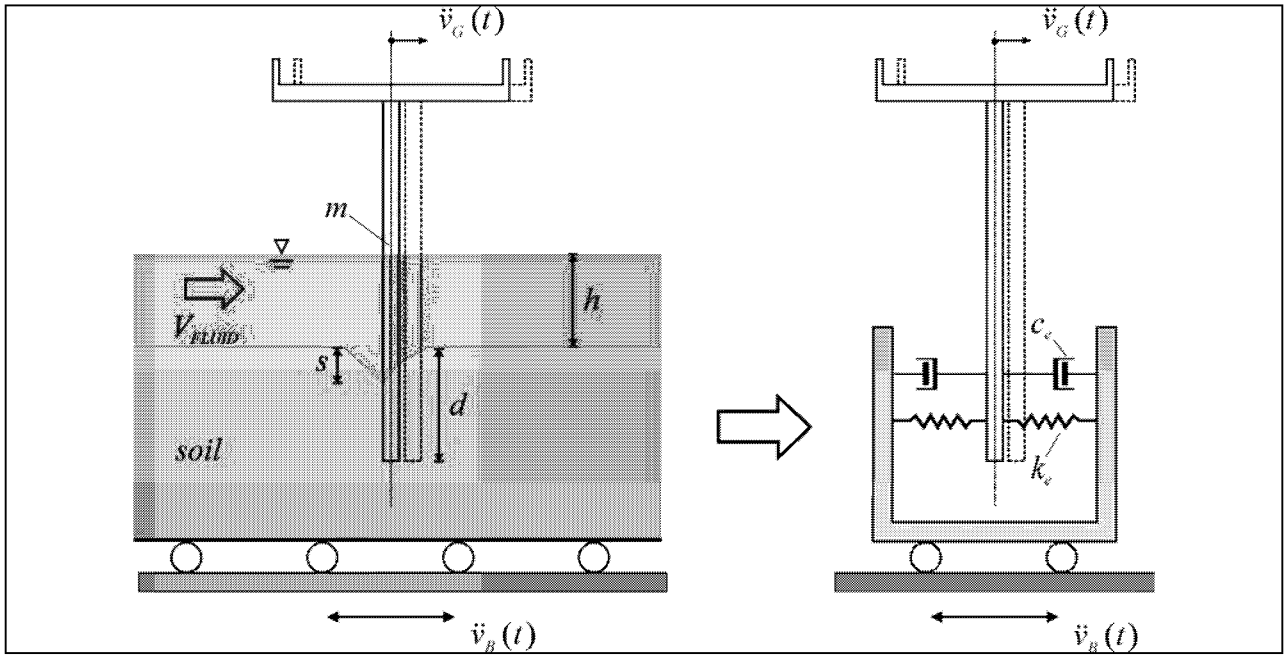

Figure 5.: Replacing fluid and soil with an equivalent spring damper system

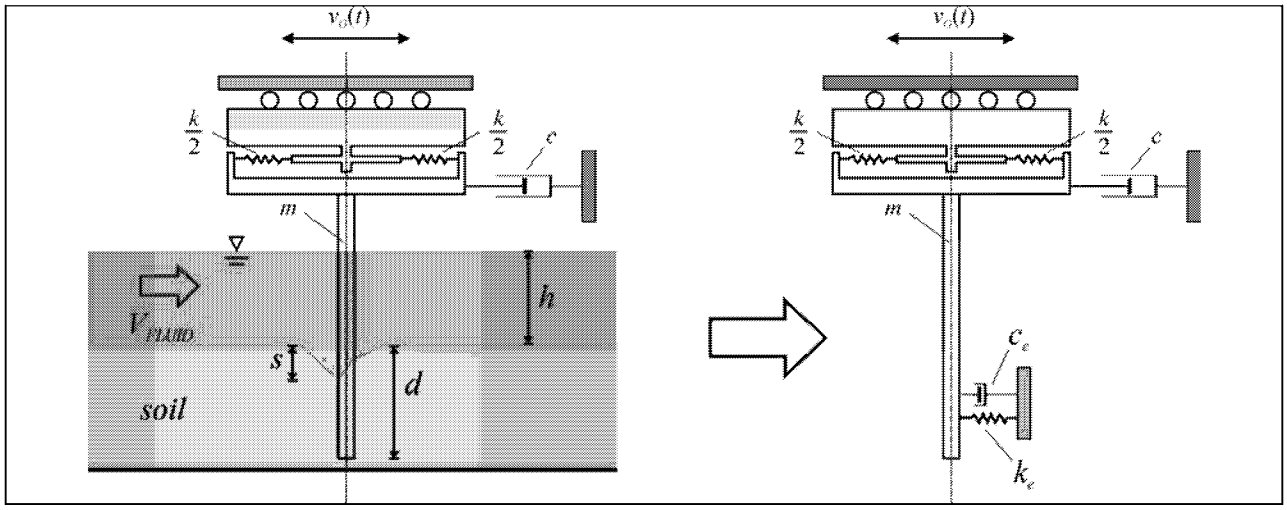

Figure 6.: Mechanical and fluid-soil subsystem considering only relative movements

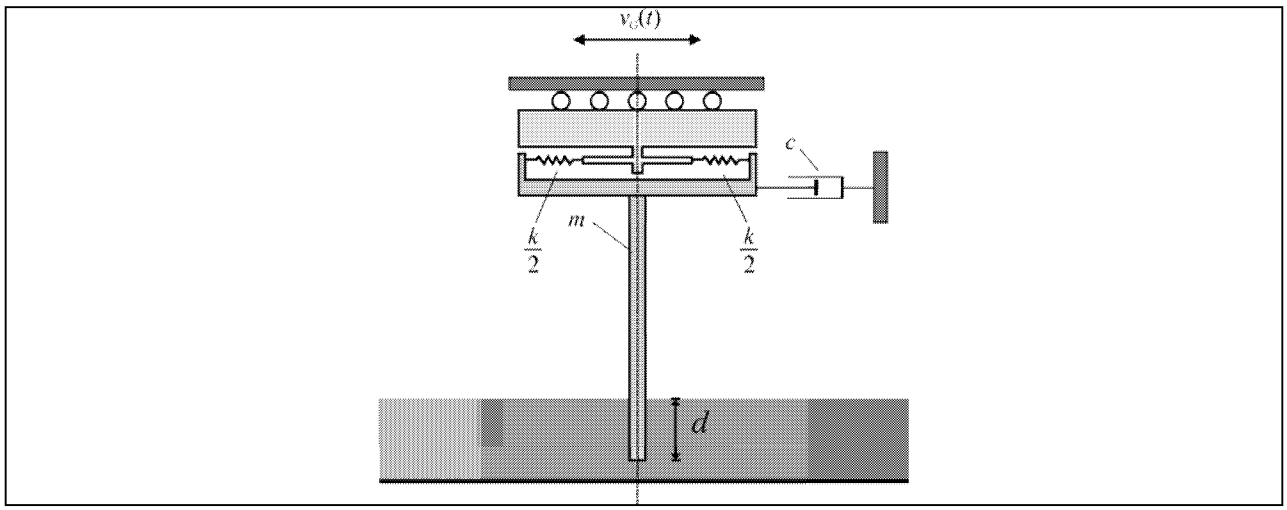

Figure 7.: Soil - Structure Interaction

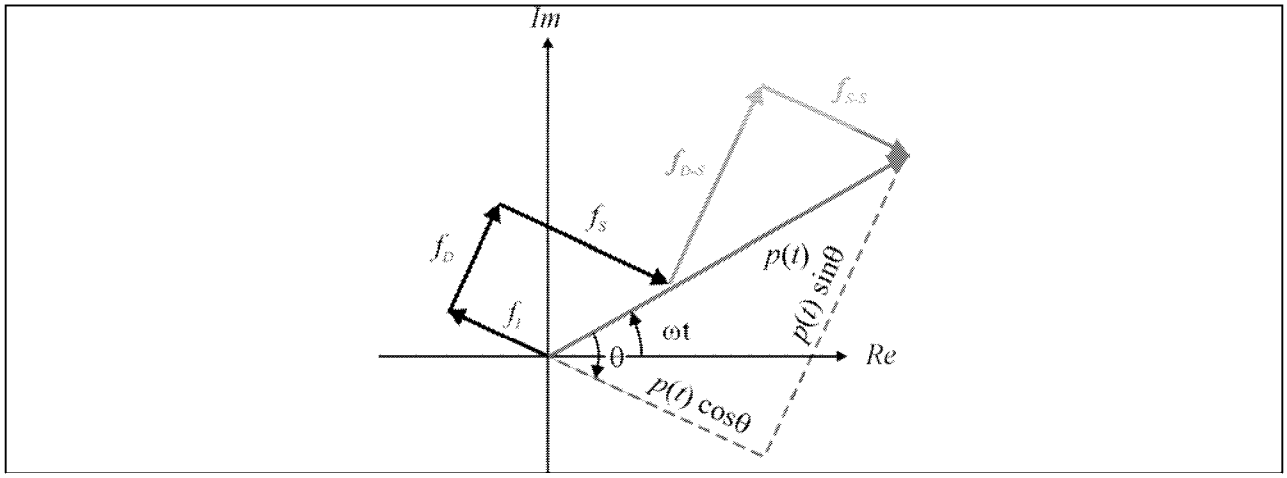

Figure 8.: SDOF system interacting with soil as a closed polygon representation in the complex plane

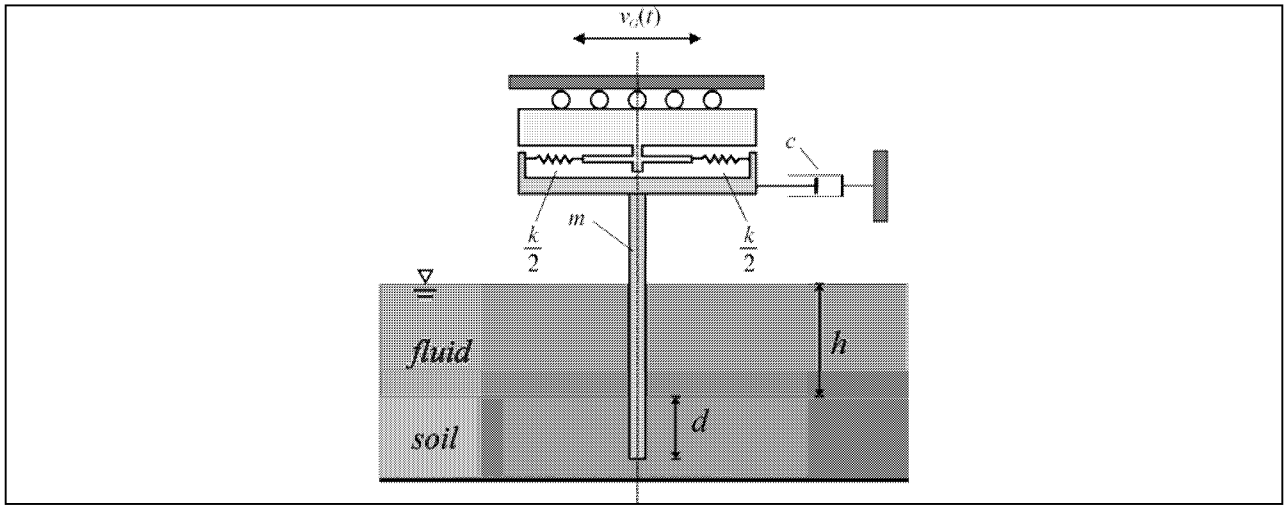

Figure 9: Fluid - Soil - Structure Interaction

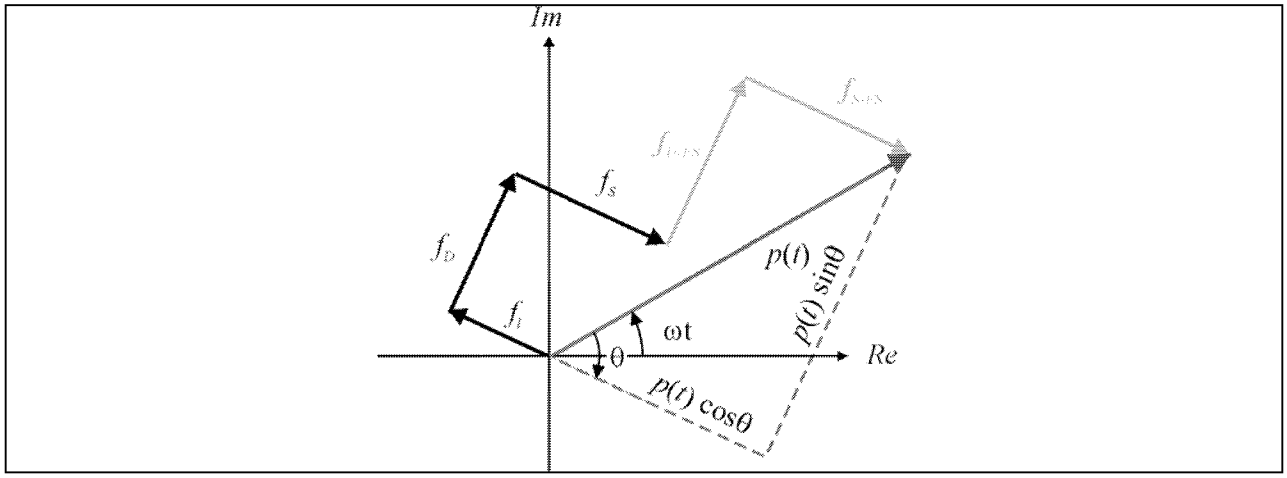

Figure 10: SDOF system interacting with fluid and soil as a closed polygon representation in the complex plane

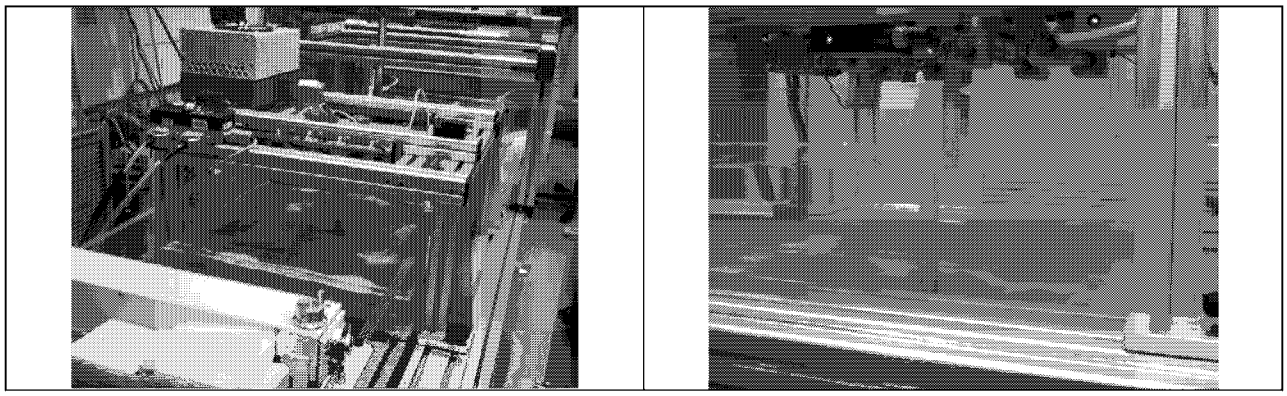

Figure 11: Shaking device and oscillating pile in fluid and soil

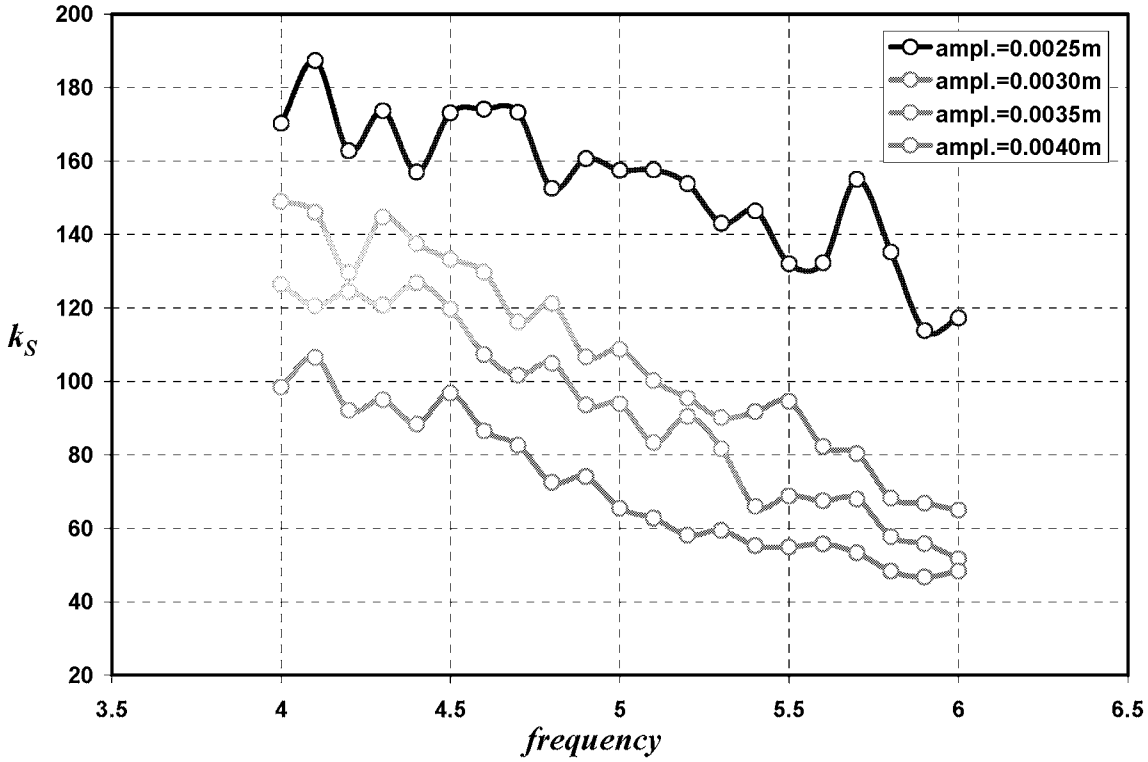

Figure 12: Soil stiffness vs. frequency for different pile amplitudes

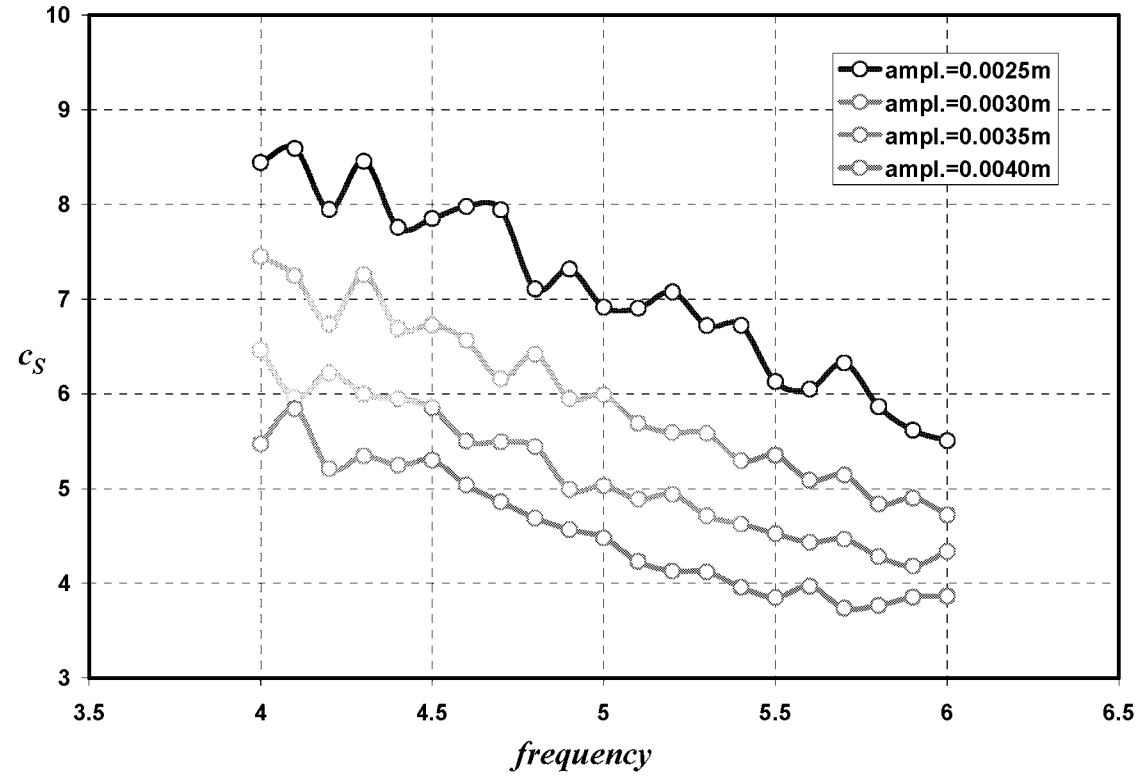

Figure 13: Soil damping vs. frequency for different pile amplitudes

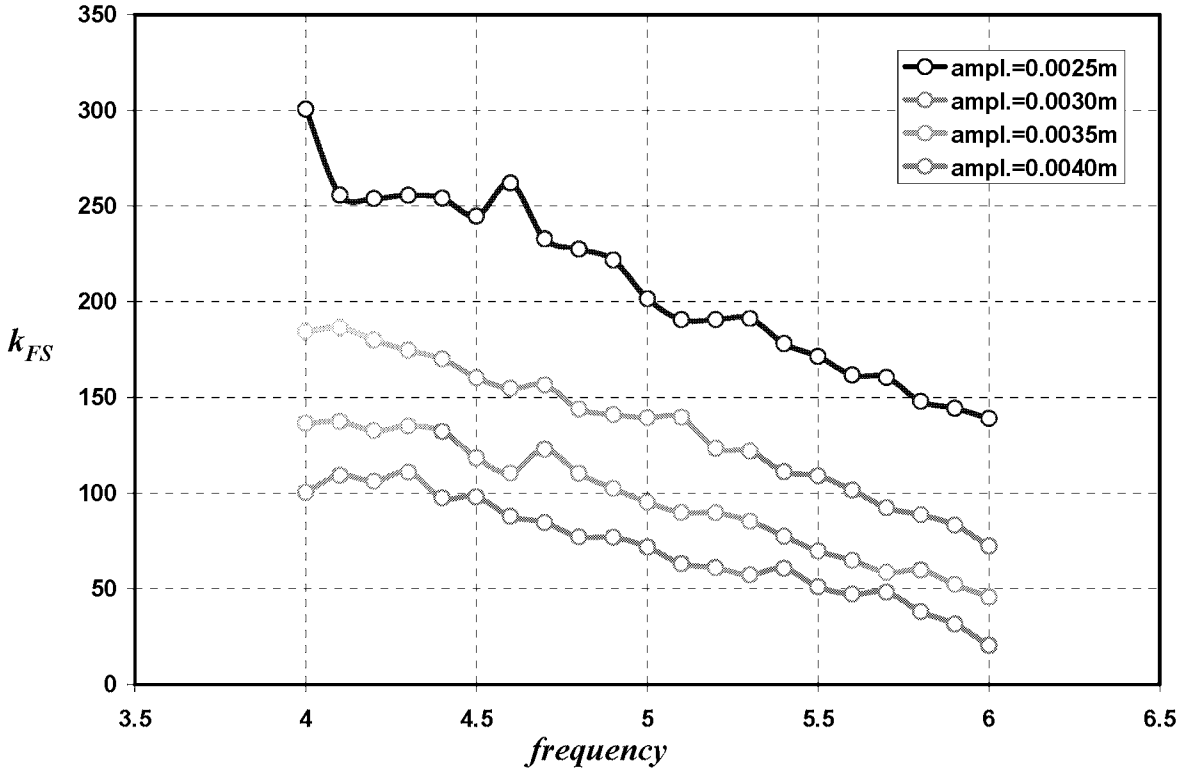

Figure 14: Fluid - Soil stiffness vs. frequency for different pile amplitudes

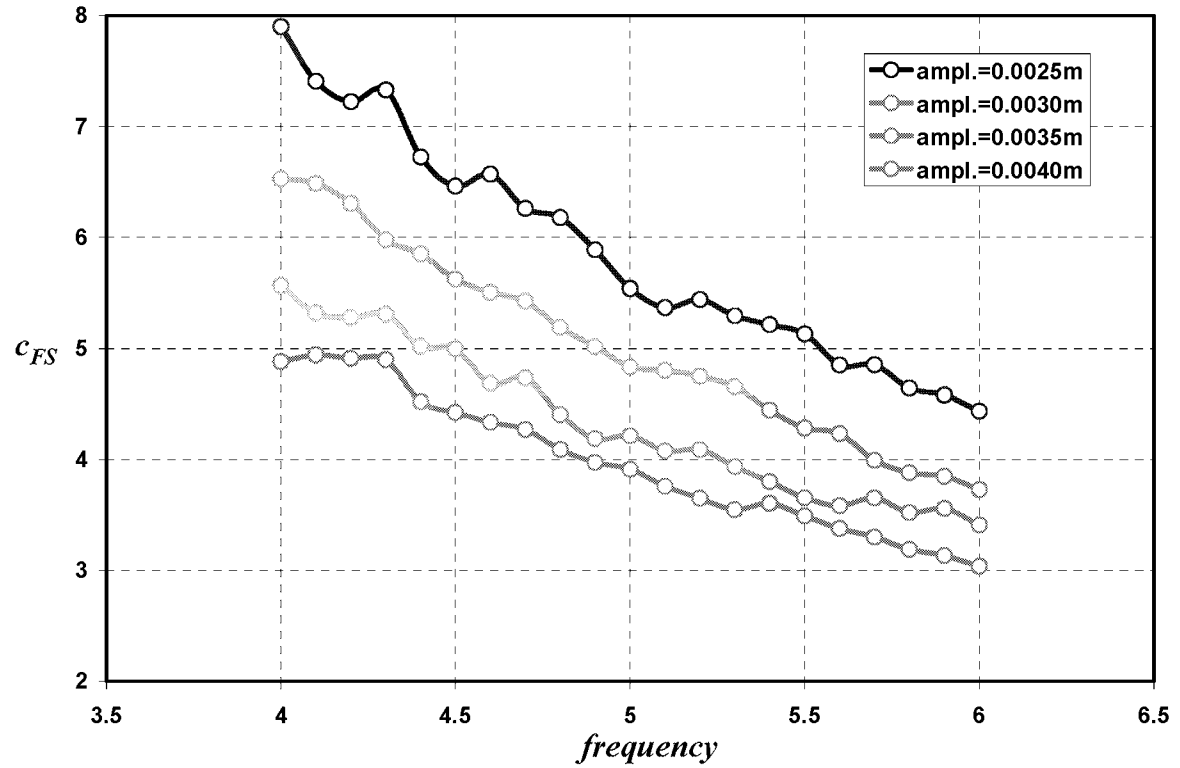

Figure 15: Fluid - Soil damping vs. frequency for different pile amplitudes